Ti_3C_2/PVDF membrane for efficient seawater desalination based on interfacial solar heating

Huan Peng, Kehang Zhu, Chenxing Li, Yangyi Xiao and Miaomiao Ye

ABSTRACT

The photothermal material of Ti_3C_2 was synthesized by etching Ti_3AlC_2 with hydrofluoric acid. The as-prepared Ti_3C_2 was deposited on a polyvinylidene fluoride (PVDF) membrane via vacuum filtration to form a Ti_3C_2/PVDF membrane, which was used for seawater desalination in the next step based on interfacial solar heating. The water evaporation rate of the Ti_3C_2/PVDF membrane could be enhanced to 0.98 kg/m^2·h under 2 sun irradiance, which was 2.8 times and 5.4 times higher than that of pure water (0.35 kg/m^2·h) and PVDF (0.18 kg/m^2·h) respectively. The temperature difference between the two air–water interfaces with and without the Ti_3C_2/PVDF membrane was as high as 11.8 °C, confirming the interfacial heating behavior. The water evaporation rate under 2 sun irradiance kept mostly in the range of 0.96–0.86 kg/m^2·h over 30 days under continuous operation, indicating the high stability of the Ti_3C_2/PVDF membrane. Finally, it was demonstrated that the typical water-quality indexes of the condensed fresh water were below the limit values of the Standards for Drinking Water Quality in China, WHO, and US EPA.

Key words | desalination, interfacial solar heating, Ti_3C_2, water evaporation

Huan Peng
Chenxing Li
Yangyi Xiao
Miaomiao Ye (corresponding author)
Zhejiang Key Laboratory of Drinking Water Safety and Distribution Technology, College of Civil Engineering and Architecture,
Zhejiang University,
Hangzhou 310058,
China
E-mail: *yemiao008@zju.edu.cn*

Kehang Zhu
Architectural & Civil Engineering Design Institute Co., Ltd,
Hangzhou 310000,
China

HIGHLIGHTS

- A Ti_3C_2/PVDF membrane was prepared by HF etching of Ti_3AlC_2 followed by vacuum deposition on PVDF membrane.
- The water evaporation rate of the Ti_3C_2/PVDF membrane could be enhanced to 0.98 kg/m^2·h, which was 2.8 times higher than that of pure water.
- The typical water-quality indexes of the condensed fresh water were below the limit values of the Standards for Drinking Water Quality in China, WHO, and US EPA.

INTRODUCTION

Water shortage has become an urgent problem around the world, restricting social progress and economic development. The contradiction between supply and demand of water resources is sharp, with current predictions that more than half of the world's population (about 3.9 billion people) will live in water-scarce areas by 2025 (Elimelech & Phillip 2011). Therefore, solving the problem of water shortage is very important for achieving sustainable development of society and improving people's living standards. Compared with the other commonly used fresh water acquisition methods, seawater desalination is considered as the most feasible and economical way to solve the shortage of water resources because 96.5% of the Earth's water resources are distributed in the ocean. The current seawater desalination technologies mainly involve reverse osmosis (RO) (Malaeb & Ayoub 2011) and

doi: 10.2166/ws.2020.298

multi-stage flash (MSF) (Khawaji *et al.* 2008). However, these two types of technologies require high energy consumption and advanced supporting infrastructure, as well as large centralized installations, which limit the application in distributed small villages or remote regions (Ghaffour *et al.* 2013).

A new concept named 'air–water interface solar heating' emerged to be applied for seawater desalination in the early 2010s (Zeng *et al.* 2011, 2014, 2015). The principle of this concept is that the transformation of water from liquid to gas only occurs on the surface of the water (Ghasemi *et al.* 2014; Zhang *et al.* 2015). Therefore, only the surface water needs to be heated instead of the whole water body to achieve desalination. Due to the poor light absorption capacity of water, light will penetrate into the solution when solar radiation falls on the water surface without materials (Zhang *et al.* 2015; Wang *et al.* 2016). This leads to inefficient photothermal conversion. Nowadays, a common method to raise the temperature of surface water is to float a layer of light absorbing material (Qiblawey & Banat 2008; Shannon *et al.* 2008) on the interface. To date, four types of photothermal materials, including plasmonic metallic nanoparticles (Zhou *et al.* 2016), metallic oxides (Wang *et al.* 2017; Ye *et al.* 2017), carbon-based materials (Li *et al.* 2016) and some unique materials have been applied to solar evaporation due to their excellent solar–thermal conversion efficiency.

Herein, we report that Ti_3C_2 is another new photothermal material because of its excellent electromagnetic wave absorption and subsequent heat generation operation (Ma *et al.* 2018; Ren *et al.* 2018). The Ti_3C_2 was synthesized by etching Ti_3AlC_2 with HF. For floating on the water surface, the Ti_3C_2 was deposited on the PVDF membrane. The PVDF membrane was used as the support for floating because of its hydrophobic surface. Moreover, the Ti_3C_2/PVDF membrane has an advantage over other photothermal materials due to its convenient separation and recycling in liquid-phase reactions. Finally, the quality of the condensed fresh water was tested for evaluating the potential application of this new seawater desalination technology. The purposes of this study are: (i) to provide a Ti_3C_2/PVDF membrane for seawater desalination based on interfacial solar heating; (ii) to examine the water quality of the condensed fresh water obtained using this technology.

Experimental section

Chemicals

All chemicals were of analytical grade and used as received without further purification. Titanium aluminum carbide (Ti_3AlC_2, 98%) was purchased from Fosman Co., Ltd. Sodium chloride, hydrogen fluoride and ethanol (99.7%) were purchased from Sinopharm. Polyvinylidene fluoride membrane was purchased from Amanda PVDF Nano Spraying Co., China.

Preparation of Ti_3C_2 and Ti_3C_2/PVDF membrane

Ti_3C_2 was prepared according to the following methods (Dong *et al.* 2016; Zhang *et al.* 2016). Typically, 0.3 g Ti_3AlC_2 powder was dissolved in a mixed solution of 20 mL ethanol and 1 mL hydrogen fluoride with magnetic stirring for 24 hours to remove the aluminum element. After etching, the mixture was constantly washed with ethanol, shaken evenly and centrifuged for each cycle, until the pH value of the supernatant increased to 7. The Ti_3C_2 was dried in an oven at 60 °C for 12 h.

The as-prepared Ti_3C_2 in different amounts ranging from 40 to 70 mg was dispersed in 50 mL of ethanol by ultrasonic crushing in a biosafer 650–92 Ultrasonic Cell Shredder at an ultrasonic power of 650 W for 5 min. Then, the Ti_3C_2 was uniformly deposited on the surface of the PVDF membrane by vacuum filtration at 0.07 MPa. Finally, the Ti_3C_2/PVDF membrane was dried in an oven at 60 °C for 12 hours.

Water evaporation

Water evaporation experiments were conducted at a temperature of 25 ± 1 °C and air humidity of 50% ± 10%. Firstly, 150 mL of water was filled in a cylindrical glass, then the Ti_3C_2/PVDF membrane was placed on the water surface. A 300 W CEL-S500 xenon lamp obtained from Beijing Zhong Jiao Jin Yuan Science and Technology Co, China, with an AM 1.5 filter was used to simulate the solar light. The light intensity can be adjusted in the range of 1,000–4,700 W/m^2, as measured by a laser power meter (LP-3A, Beijing Physcience Opto-Electronics, China). The weight

of the evaporated water was measured using an electronic balance (FA2104, Shanghai Sunny Hengping Scientific Instrument Co., Ltd).

Materials characterization and water-quality analysis

The crystalline properties of the Ti_3C_2 and Ti_3AlC_2 were identified by an X-ray diffractometer (XRD, Rigaku, Japan) using Cu Kα radiation (45 kV, 40 mA). The morphologies of Ti_3C_2 and Ti_3AlC_2 were examined by an FEI FEG650 field-emission scanning electron microscope and a JEM 2010 transmission electron microscope (TEM) at an accelerating voltage of 200 kV. The contact angle of the Ti_3C_2/PVDF membrane was measured by an OCA20 contact angle measuring device (Dataphysics, Germany). A U-4100 ultraviolet-visible-near-infrared (UV-Vis-NIR) spectrophotometer (Hitachi, Japan) in which $BaSO_4$ powder was used as the 100% reflectance standard and an integrating sphere accessory was equipped to obtain UV-Vis-NIR diffuse reflectance spectra of the Ti_3C_2 and Ti_3AlC_2. The temperature of the Ti_3C_2/PVDF membrane surface was supervised by an IR camera (FTIR T650sc, USA). The concentration of anions and cations in the condensed fresh water were examined by a Dionex ICS-2000 ion chromatograph (Dionex, USA) and a PE NexION 300Q inductively coupled plasma mass-spectrometer (Perkin Elmer, USA), respectively. Excitation-emission matrix (EEM) fluorescence spectroscopy was performed by a fluorescence regional integration (FRI) method (HITACHI-F 4600, Japan).

RESULTS AND DISCUSSION

Synthesis and characterization of Ti_3C_2

In order to verify whether aluminum was completely etched by HF, the crystalline structures of the Ti_3C_2 before and after HF etching were analyzed by X-ray diffraction. The diffraction peaks originating from the Al element in the Ti_3AlC_2 sample (Figure 1(a)) almost disappeared after HF etching, indicating that the Al element was gradually decreased. The morphologies of the Ti_3C_2 before and after HF etching were examined by SEM and TEM observation. Before HF etching, a distinct dense layered structure with a thickness of about 0.3 μm can be clearly observed in the pristine Ti_3AlC_2 (Figure 1(b) and 1(e)). After HF etching, Ti_3C_2 was obviously peeled off from the layered structure to form a single smooth plate crystal with a length of 3.0 μm and a width of 1.4 μm (Figure 1(c) and 1(f)). It can be seen that the gap between the Ti_3C_2 particles increased, which is conducive for vapor to pass through, resulting in enhanced water yield. Moreover, a single flaky crystal can also reduce the dosage of Ti_3C_2 needed for desalination.

The optical absorption property, which is one of the important properties of the photothermal conversion

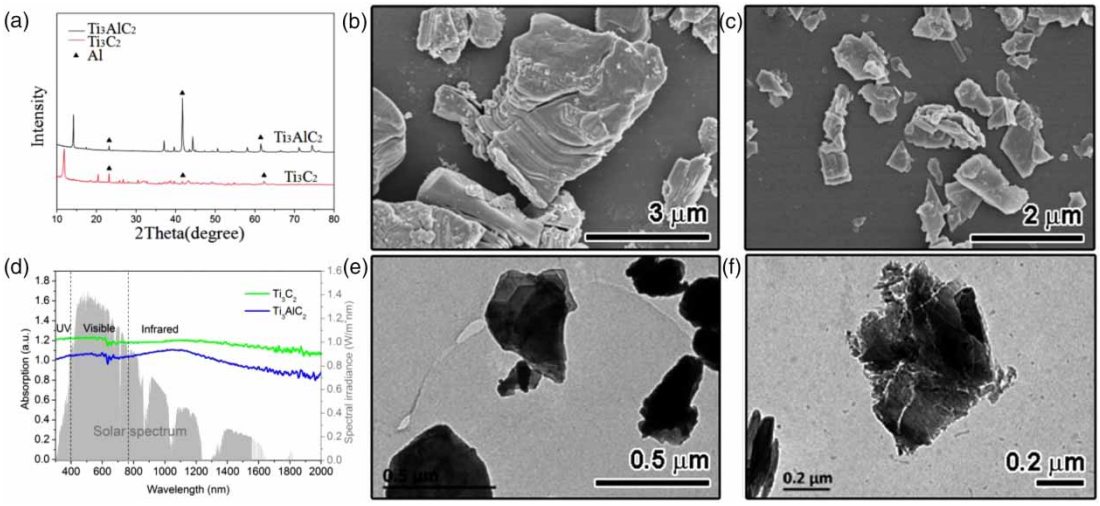

Figure 1 | (a) XRD patterns and (d) UV-Vis-NIR diffuse reflectance spectra of the Ti_3AlC_2 and Ti_3C_2; SEM images of (b) Ti_3AlC_2 and (c) Ti_3C_2; TEM images of (e) Ti_3AlC_2 and (f) Ti_3C_2.

material, was primarily investigated. Ti_3AlC_2 and Ti_3C_2 were both deposited on PVDF membrane for measurement. Clearly, the absorption of the materials spans from the ultraviolet (<400 nm) to the visible (400–760 nm) and near-infrared (760–2,200 nm) spectral regions, indicating their great potential in solar energy conversion applications (Figure 1(d)). The light absorption proportion in different spectrum regions in the wavelength range from 400 to 2,200 nm can be calculated by the MATLAB software according to the following equation (Zhang *et al.* 2015):

$$A = \frac{\int (1 - R) \cdot S \cdot d\lambda}{\int S \cdot d\lambda} \quad (1)$$

Here, A, R, S and λ represent solar absorption, sample reflectivity, solar spectral irradiance (W/m^2·nm), and wavelength (nm), respectively; $(1 - R)\cdot S$ represents the sample absorption of solar spectral irradiance. As calculated, the solar absorption of the Ti_3C_2 from the ultraviolet (<400 nm) to the visible (400–760 nm) and near-infrared (760–2,200 nm) was 4.38%, 47.65%, and 44.33%, respectively. Correspondingly, the solar absorption of Ti_3AlC_2 in the ultraviolet, visible and near-infrared regions was 4.07%, 45.75% and 43.10%, respectively. Thus, the total solar absorption of Ti_3AlC_2 and Ti_3C_2 is 92.92% and 96.36% respectively. The slightly enhanced solar absorption is probably due to the sheet-like morphology of Ti_3C_2, which has the larger light-absorbing surface area (Xu *et al.* 2017).

As shown in the digital photo (Figure 2(a)), the Ti_3C_2/PVDF membrane has a smooth surface. In addition, 3D optical microscopy analysis was carried out to further measure the thickness and surface property of the Ti_3C_2/PVDF membrane. As measured (Figure 2(b)), the heights of the highest point and the lowest point of the Ti_3C_2/PVDF membrane differed by 41.65 μm, and the average thickness was 21.34 μm. The surface of the Ti_3C_2/PVDF was smooth and flat, which ensures that the Ti_3C_2 can be heated uniformly under the solar light while avoiding the surface structure damage caused by local high temperature. In order to float on the water surface, the Ti_3C_2 was deposited on the surface of the hydrophobic PVDF membrane. The hydrophobicities of the PVDF and Ti_3C_2/PVDF membrane were characterized by measuring the water contact angle. The contact angles of PVDF (Figure 2(c)) and the Ti_3C_2/PVDF membrane (Figure 2(d)) were 136.5° and 128.6° respectively, which indicate the hydrophobic surface of the Ti_3C_2/PVDF membrane. As a result, the Ti_3C_2/PVDF membrane can be easily floated on the water surface due to the surface tension effect.

Water evaporation

The performance of the Ti_3C_2/PVDF membrane for water evaporation was explored. As references, water evaporation

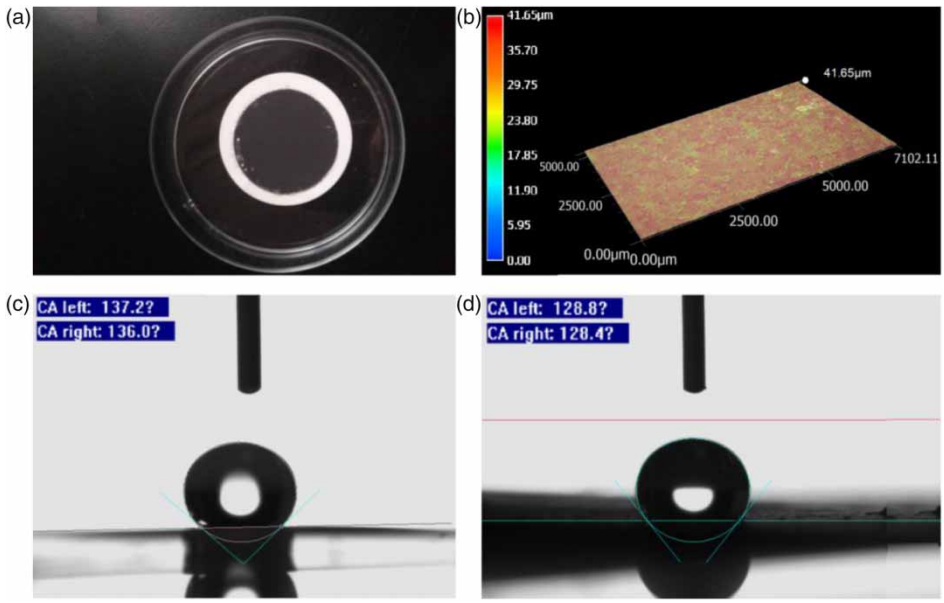

Figure 2 | (a) Digital photo and (b) 3D optical microscopy image of Ti_3C_2/PVDF membrane. Contact angle of (c) PVDF membrane and (d) Ti_3C_2/PVDF membrane.

by PVDF membrane and evaporation of pure water itself were also conducted. As can be seen in Figure 3(a), all water evaporation processes can be simply modeled using zero-order kinetics, which can be described as:

$$m - m_0 = kt \tag{2}$$

where k is the water evaporation rate, m_0 is the initial water mass, and m is the actual water mass at time t. The k value of Ti_3C_2/PVDF membrane was 0.98 kg/m^2·h, which was 2.8 times and 5.4 times higher than pure water (0.35 kg/m^2·h) and PVDF (0.18 kg/m^2·h) respectively. The enhanced water evaporation rate of the Ti_3C_2/PVDF membrane clearly proves that Ti_3C_2/PVDF membrane can enable effective interfacial solar heating and promote water evaporation. The decreased k value of the PVDF was due to the hydrophobicity and light reflection effect of PVDF membrane.

The temperature change of the air–water interface can further confirm the heating effect of the Ti_3C_2/PVDF membrane on the solar interface. Before solar irradiation, the temperature of the air–water interface with and without Ti_3C_2/PVDF film measured by infrared thermal imager was 21.2 and 22.1 °C, respectively (Figure 4). The surface temperature of the Ti_3C_2/PVDF membrane was raised to 43.3 °C, which was 11.8 °C higher than the pure water after only ten minutes of solar irradiance. It can be seen from the temperature change curve that the temperature rise of the pure water was relatively balanced throughout the water body, while the temperature rose rapidly within the first ten minutes after floating a Ti_3C_2/PVDF membrane on the water surface. After being irradiated for 60 minutes, the surface temperature of the Ti_3C_2/PVDF membrane reached a steady state. This was because a large amount of water evaporated and took away heat, making the temperature stable at 48 °C.

In order to optimize the solar evaporation conditions, the effects of Ti_3C_2 dose and solar irradiance intensity were investigated, and the results are shown in Tables 1 and 2. The water evaporation rate (k) increased from 0.59 to 0.98 kg/m^2·h with increase of Ti_3C_2 dose from 40 to 60 mg. Further increasing the Ti_3C_2 dose to 70 mg resulted in a deterioration of the k value (Figure 3(b)), which can be attributed to the excessive

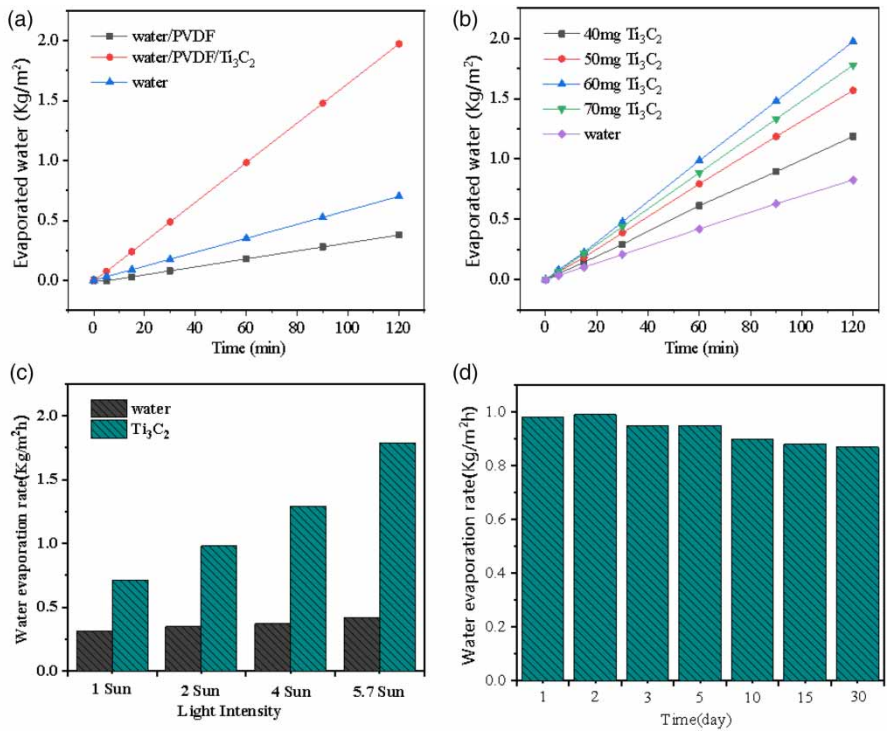

Figure 3 | (a) The mass of the evaporated water in PVDF membrane, Ti_3C_2/PVDF membrane and pure water versus the irradiation time. The effects of (b) Ti_3C_2 dose and (c) solar light intensity on the water evaporation rate. (d) Water evaporation rate of Ti_3C_2/PVDF membrane under 2 sun solar irradiance over 30 days.

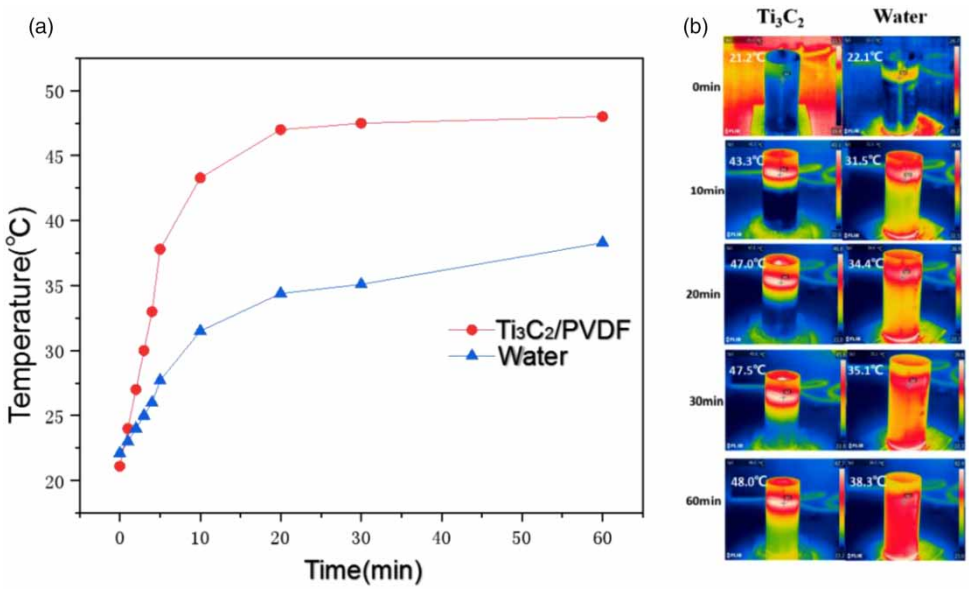

Figure 4 | (a) The temperature change of the water surface over time; (b) the IR images with and without Ti_3C_2/PVDF membrane at different times.

Table 1 | The effect of Ti_3C_2 dose on water evaporation rate

Ti_3C_2 dose (mg)	Zero-order kinetic equation	Water evaporation rate (kg·m^{-2}·min^{-1})	Water evaporation rate (kg·m^{-2}·h^{-1})	R^2
40	$y = 0.00983x + 0.00037$	0.00983	0.59	0.9986
50	$y = 0.01300x - 0.00989$	0.01300	0.78	0.9898
60	$y = 0.01633x - 0.00788$	0.01633	0.98	0.9998
70	$y = 0.01487x - 0.00605$	0.01487	0.89	0.9934
water	$y = 0.00581x + 0.00164$	0.00581	0.35	0.9998

Table 2 | The effect of solar light intensity on water evaporation rate

Number	Zero-order kinetic equation	Water evaporation rate (kg·m^{-2}·min^{-1})	Water evaporation rate (kg·m^{-2}·h^{-1})	R^2
1	$y = 0.00521x - 0.00249$	0.00521	0.31	0.9941
2	$y = 0.01183x - 0.00571$	0.01183	0.71	0.9932
3	$y = 0.00589x - 0.00281$	0.00589	0.35	0.9838
4	$y = 0.01633x - 0.00788$	0.01633	0.98	0.9998
5	$y = 0.00622x - 0.00298$	0.00622	0.37	0.9859
6	$y = 0.02150x - 0.01037$	0.02150	1.29	0.9925
7	$y = 0.00708x - 0.00338$	0.00708	0.42	0.9946
8	$y = 0.02983x - 0.01439$	0.02983	1.79	0.9947

Water evaporation under (1#) 1 sun, (3#) 2 sun, (5#) 4 sun, (7#) 5.7 sun irradiance.
Water evaporation with PVDF/Ti_3C_2 under (2#) 1 sun, (4#) 2 sun, (6#) 4 sun, (8#) 5.7 sun irradiance.

photothermal materials that hindered vapor transport velocity. The effects of the light intensities on the water evaporation rate were investigated by tuning the light intensity in the range from 1 to 5.7 sun while keeping other evaporation conditions unchanged. With the increase of light intensity, the water evaporation rates of the pure water just increased from 0.31 to

0.42 kg/m^2·h, which was probably due to the specular reflection of the water surface (Figure 3(c)). However, after covering with a thin Ti_3C_2/PVDF membrane, the water evaporation rates were correspondingly enhanced to 0.71, 0.98, 1.29 and 1.79 kg/m^2·h under 1, 2, 4 and 5.7 sun, which was 2.29, 2.81, 3.49 and 4.26 times that of the corresponding pure water respectively. This experiment further confirms that Ti_3C_2 has good heat absorption and interface heating effects.

For their long-term stable operation and future commercial applications, durability and stability are very important properties because they can reduce costs if they allow reuse. Figure 3(d) shows the water evaporation rate of the floating Ti_3C_2/PVDF membrane under 2 sun for different periods of 1, 2, 3, 5, 10, 15, 30 days. With the increase of time, the water evaporation rate decreased slightly, but it was stable in the range of 0.96–0.86 kg/m^2·h. A difference in water evaporation rate was not evident over the 30-day measured period, revealing the good stability and durability of the Ti_3C_2/PVDF membrane.

To further evaluate the quality of the condensed fresh water obtained by the Ti_3C_2/PVDF membrane, a real seawater sample obtained from the East China Sea was used as the source water for solar evaporation. Water-quality indexes including conductivity, turbidity, cations and anions of the East China Sea water before and after solar distillation by Ti_3C_2/PVDF membrane were investigated. The conductivity (salinity) of the seawater was significantly reduced from 36,400 to 16.8 μs/cm (Figure 5(a)), which is far below the value (2,500 μs/cm) defined by WHO. As an important test item in drinking water standards, the turbidity of the seawater was significantly reduced from 6.07 NTU to 0.63 NTU, which is far below the value (5 NTU) defined by WHO (Figure 5(b)). Other typical cations and anions such as Na^+, K^+, Ca^{2+}, Mg^{2+}, SO_4^{2-}, NO_3^-, Cl^-, F^- and Br^- decreased to <0.01–1.91 mg/L (as shown in Table 3), which are all below the drinking standard defined by the World Health Organization (WHO), the Standards for Drinking Water Quality in China and the US Environmental Protection Agency (EPA).

Table 3 | Typical water-quality indexes of the East China Sea water before and after solar distillation by Ti_3C_2/PVDF membrane

Cations or anions	Seawater (mg/L)	Distilled water (mg/L)
F^-	0.956	0.015
Cl^-	15,134	1.91
NO_3^-	5.74	0.013
SO_4^{2-}	2,043.02	0.85
Br^-	43.34	0.51
Na^+	6,543.71	0.35
K^+	259.53	<0.01
Ca^{2+}	317.67	0.21
Mg^{2+}	854.85	0.15

Besides the inorganic items, organic items as total organic carbon (TOC) were also investigated. The TOC concentration (Figure 5(c)) was reduced from 3.85 to 0.79 mg/L, which is lower than the value defined by China's drinking water-quality standard (GB5749-2006). Excitation–emission matrix (EEM) fluorescence spectroscopy was employed to further analyze the types of organic compounds. Different kinds of organics are located in different regions of the fluorescence spectrum. The lower the fluorescence response value, the lower the organic content. Comparing Figure 6(a) with Figure 6(b), it can be found that the distillation of the East China Sea without adding materials will greatly increase the concentration of organic matter in condensed fresh water. This is because the organic matter in the

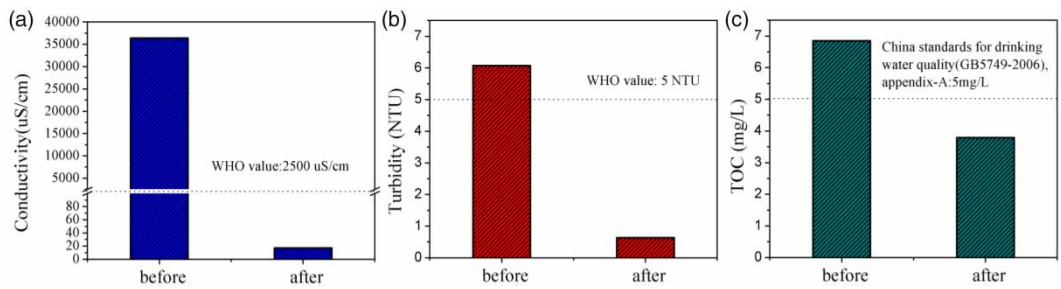

Figure 5 | (a) Conductivity, (b) turbidity and (c) TOC in seawater and condensed fresh water.

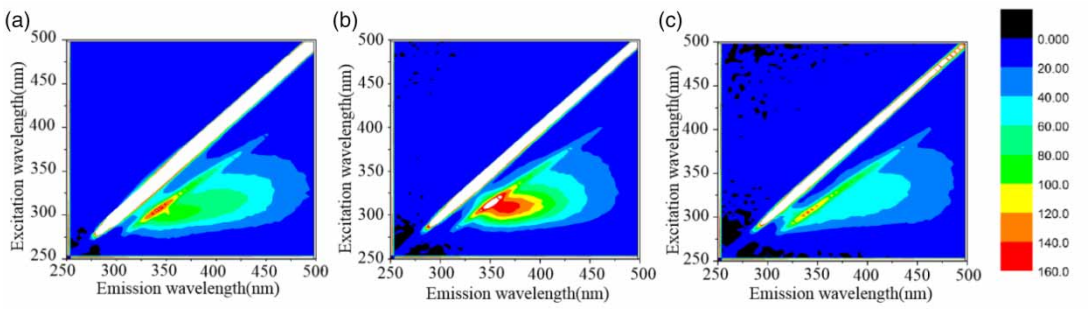

Figure 6 | 3D fluorescence diagrams of (a) East China Sea water, and condensed fresh water obtained (b) without and (c) with Ti_3C_2/PVDF membrane.

seawater is also volatile, thus the organic matter will evaporate together with the evaporation of water. However, after adding Ti_3C_2/PVDF membrane (Figure 6(c)), the organic matter in the condensed fresh water will be lower than that of the original East China Sea, which shows that the Ti_3C_2 has a very significant adsorption and removal property on for organic matter removal.

CONCLUSION

In summary, a Ti_3C_2/PVDF membrane was prepared by HF etching of Ti_3AlC_2 followed by vacuum deposition on a hydrophobic PVDF membrane surface. An enhanced water evaporation rate was achieved due to high solar absorption, uniform heating of the Ti_3C_2/PVDF membrane, and the interfacial solar heating effect. In addition, the enhanced water evaporation rate, the encouraging durability and stability, as well as the high quality of the condensed fresh water make the Ti_3C_2/PVDF membrane potentially useful in islands with insufficient fresh water supply.

ACKNOWLEDGEMENTS

The present work was financially supported by the National Natural Science Foundation of China (No. 52070161 and No. 51761145022), the Public Welfare Technology Application Research Project of Zhejiang Province (No. LGG18E080002), the National Science and Technology Major Protects for Water Pollution Control and Treatment (No. 2017ZX07201004), and the Fundamental Research Funds for the Central Universities (No. 2018FZA4017).

DATA AVAILABILITY STATEMENT

All relevant data are included in the paper or its Supplementary Information.

REFERENCES

Dong, S. Y., Shen, L. F., Li, H. S., Pang, G., Dou, H. & Zhang, X. G. 2016 Flexible sodium-ion pseudocapacitors based on 3D $Na_2Ti_3O_7$ nanosheet arrays/carbon textiles anodes. *Advanced Functional Materials* **26** (21), 3703–3710.

Elimelech, M. & Phillip, W. A. 2011 The future of seawater desalination: energy, technology, and the environment. *Science* **333** (6043), 712–717.

Ghaffour, N., Missimer, T. M. & Amy, G. L. 2013 Technical review and evaluation of the economics of water desalination: current and future challenges for better water supply sustainability. *Desalination* **309**, 197–207.

Ghasemi, H., Ni, G., Marconnet, A. M., Loomis, J., Yerci, S., Miljkovic, N. & Chen, G. 2014 Solar steam generation by heat localization. *Nature Communications* **5**, 4449.

Khawaji, A. D., Kutubkhanah, I. K. & Wie, J. M. 2008 Advances in seawater desalination technologies. *Desalination* **221** (1–3), 47–69.

Li, X. Q., Xu, W. C., Tang, M. Y., Zhou, L., Zhu, B., Zhu, S. N. & Zhu, J. 2016 Graphene oxide-based efficient and scalable solar desalination under one sun with a confined 2D water path. *National Academy of Sciences of the United States of America* **113** (49), 13953–13958.

Ma, Z. Y., Zhou, X. F., Deng, W., Lei, D. & Liu, Z. P. 2018 3D porous MXene (Ti_3C_2)/reduced graphene oxide hybrid films for advanced lithium storage. *ACS Applied Materials & Interfaces* **10** (4), 3634–3643.

Malaeb, L. & Ayoub, G. M. 2011 Reverse osmosis technology for water treatment: state of the art review. *Desalination* **267** (1), 1–8.

Qiblawey, H. M. & Banat, F. 2008 Solar thermal desalination technologies. *Desalination* **220** (1–3), 633–644.

Ren, C. E., Alhabeb, M., Byles, B. W., Zhao, M. Q., Anasori, B., Pomerantseva, E., Mahmoud, K. A. & Gogotsi, Y. 2018 Voltage gated ions sieving through 2D MXene $Ti_3C_2T_x$ membranes. *ACS Applied Nano Materials* **1** (7), 3644–3652.

Shannon, M. A., Bohn, P. W., Elimelech, M., Georgiadis, J. G., Mariñas, B. J. & Mayes, A. M. 2008 Science and technology for water purification in the coming decades. *Nature* **452** (7185), 301–310.

Wang, Y. C., Zhang, L. B. & Wang, P. 2016 Self-floating carbon nanotube membrane on macroporous silica substrate for highly efficient solar-driven interfacial water evaporation. *ACS Sustainable Chemistry & Engineering* **4** (3), 1223–1230.

Wang, J., Li, Y. Y., Deng, L., Wei, N. N., Weng, Y. K., Dong, S., Qi, D. P., Qiu, J., Chen, X. D. & Wu, T. 2017 High-performance photothermal conversion of narrow-bandgap Ti_2O_3 nanoparticles. *Advanced Materials* **29** (3), 1603730.

Xu, N., Hu, X. Z., Xu, W. C., Li, X. Q., Zhou, L., Zhu, S. N. & Zhu, J. 2017 Mushrooms as efficient solar steam-generation devices. *Advanced Materials* **29** (28), 1606762.

Ye, M. M., Jia, J., Wu, Z. J., Qian, C. X., Chen, R., O'Brien, P. G., Sun, W., Dong, Y. C. & Ozin, G. A. 2017 Synthesis of black TiO_x nanoparticles by Mg reduction of TiO_2 nanocrystals and their application for solar water evaporation. *Advanced Energy Materials* **7** (4), 1601811.

Zeng, Y., Yao, J. F., Horri, B. A., Wang, K., Wu, Y. Z., Li, D. & Wang, H. T. 2011 Solar evaporation enhancement using floating light-absorbing magnetic particles. *Energy & Environmental Science* **4** (10), 4074–4078.

Zeng, Y., Wang, K., Yao, J. F. & Wang, H. T. 2014 Hollow carbon beads for significant water evaporation enhancement. *Chemical Engineering Science* **116**, 704–709.

Zhang, L. B., Tang, B., Wu, J. B., Li, R. Y. & Wang, P. 2015 Hydrophobic light-to-heat conversion membranes with self-healing ability for interfacial solar heating. *Advanced Materials* **27** (33), 4889–4894.

Zhang, C. F., Kim, S. J., Ghidiu, M., Zhao, M. Q., Barsoum, M. W., Nicolosi, V. & Gogotsi, Y. 2016 Layered orthorhombic Nb_2O_5@$Nb_4C_3T_x$ and TiO_2@$Ti_3C_2T_x$ hierarchical composites for high performance Li-ion batteries. *Advanced Functional Materials* **26** (23), 4143–4151.

Zhou, L., Tan, Y. L., Wang, J. Y., Xu, W. C., Yuan, Y., Cai, W. S., Zhu, S. N. & Zhu, J. 2016 3D self-assembly of aluminium nanoparticles for plasmon-enhanced solar desalination. *Nature Photonics* **10** (6), 393–398.

First received 31 July 2020; accepted in revised form 20 October 2020. Available online 5 November 2020